CALCULATION OF THREE-PHASE RELATIVE PERMEABILITIES FROM DISPLACEMENT EXPERIMENTS WITH MEASUREMENTS OF IN-SITU SATURATION

O.O. Eleri , A. Graue, A. Skauge, and J. A. Larsen
University of Bergen, Bergen, Norway

Abstract

Unsteady state coreflood experiments in a water wet Clashach core have been used to calculate three-phase oil, water and gas relative permeabilities. From the experimental results the following observations were made; relative permeabilities to the oil and gas phase depend on more than one phase saturation, hysteresis from increasing and decreasing saturations was most pronounced for the oil phase. By using an optimization algorithm relative permeabilities and capillary pressure have been simultaneously estimated from data gathered during two-phase displacements. The importance of in-situ saturation information in relative permeability determination is demonstrated in this paper.

Introduction

This work involves effects of saturation history on two- and three-phase relative permeabilities. Also the residual oil saturation acquired from series of dynamic displacements involving water, oil, and gas in a strongly water-wet medium have been analysed. The displacements have been performed by injection of one phase and thereby reducing the other phases to residual saturations. Different methods have been compared in the calculation of the relative permeabilities.

A problem with all unsteady state or displacement type of experiments is that end-effects may influence saturation distribution, effluent production, endpoint saturation and also the pressure drop along the core. Large errors in the calculated relative permeabilities may be due to flow pattern which differs from the basic assumptions made in deriving the analytical equations for relative permeability determination. In the experiments reported the distribution of all three phases are measured. The experiments allow to match both frontal movement and saturation distribution in addition to the conventional measurements of differential pressure and effluent production. The aim of this paper has been to investigate the impact of experimental conditions and restrictions on two- and three-phase relative permeability obtained by an analytical and an optimization approach.

Fluid saturation and saturation distributions were determined by an in-situ nuclear tracer imaging technique. This method had been evaluated in our earlier work[1-4] and have been found suitable for three-phase flow studies[3,4]. Gamma-emitting radioactive tracers were used to label both the brine phase and the oil phase. The gas phase saturation was calculated from material balance. The operational principle and procedure for determining in-situ fluid saturation by the nuclear tracer imaging technique has been described earlier[1,2].

Materials and Methods

Core Material and Fluids

The Clashach sandstone outcrop core (length 9.44 cm and diameter 5.17 cm) used in this work is well sorted with an average grain size of 0.25 mm. Pore throat sizes are in the range of 1 to 45 μm of which about 78% range between 18 to 28 μm. The pore volume was measured after the core had been evacuated and saturated with inactive brine. In order to saturate adsorption sites and to stabilize the permeability, about 18 pore volumes of inactive brine was injected before the absolute permeability was measured. The average value was 234 md. The core was mounted inside a Hassler-type coreholder under a confinement pressure of 40 bars and then positioned horizontally on a flow-rig. The fluids used in the displacements were brine of 5% by weight NaCl, n-decane and nitrogen gas. The brine was tagged with radioactive ^{22}NaCl tracer (activity: 1.0 mCi/l). The oil was tagged with radioactive ^{59}Fe tracer in the form of ferrocene. The ferrocene was produced by synthesis (activity: 1.5 mCi/l). The nitrogen gas used was from a commercially compressed N_2-cylinder. To avoid mass transfer of components, the injected radioactive brine or radioactive oil was saturated with nitrogen gas before injection through a transfer vessel under backpressure.

Experimental Procedure

The basic experimental set-up for the relative permeability measurements is described in Reference 2, albeit the following modifications: Brine or oil was injected through a dual piston pump which supplies pulsefree constant flowrates. Nitrogen gas was injected through a flowrate regulator which ensured constant differential pressure over the core. Produced fluids were directed to an inverted graduated cylinder where the volumes of gas and liquids were measured. The graduated cylinder was placed at the same level as the core. A differential pressure transducer incorporated with the data logging unit was used to measure the pressure drop across the core. The transducer line was bled of gas at the end of each flow sequence and recalibrated. The core was scanned before, during (depending on the duration of the flow experiment) and after each flood cycle.

Relative Permeability Measurements

Prior to the start of the relative permeability experiments, the inactive brine inside the core was miscibly displaced by radioactive brine. The flowrate was 0.25 cc/min. A mineral oil was used to drain the radioactive brine to irreducible saturation at which point the oil was miscibly displaced by ^{59}Fe tracer tagged n-decane. The drainage flowrate was 0.25 cc/min. The drainage was followed by cycles of injection of either brine, oil or gas until production of the other phases ceased. To minimize end effects and saturation gradients a high flowrate was used for a short period of time at the end of a water or oil injection cycle. Thereafter, a low rate flood was continued in order to determine the relative permeability endpoint for the injected phase. Details of the displacement cycles together with the initial and final fluid saturations, and the relative permeability endpoint for the injected phase are outlined in Table 1. W1 in the table denotes primary injection of water. G2 denotes gas injection and that this gas injection was the second in the sequence of injections, and so on. The first waterflood ,W1, was started with a flowrate of 0.1 cc/min, but following a review of the saturation profiles, it was decided to use a flowrate of 3.0 cc/min in subsequent waterfloods and oilfloods in order to satisfy the Rapoport and Leas' scaling criteria[5]. For the gasfloods, a constant differential pressure gradient of 2 bars/meter was used. The use of constant pressure gradient was to minimize frontal instability. After the waterflood, W10, gas was removed from the core by prolonged draining with mineral oil under high pressure.

The core was returned to a state similar to pre-W1 waterflood. The three-phase water-oil-gas relative permeabilities were calculated by the method of Virnovsky[6]. This method has been applied in several relative permeability studies[7-10].

Single-Phase and Two-Phase Displacements

Figure 1 shows the saturation profiles generated when the resident inactive brine was miscibly displaced by radioactive ^{22}Na tracer tagged brine. A highly dispersed displacement front was observed. Radioactive brine breakthrough occurred after more than 0.44 PV of injected fluid. After the displacement of the radioactive brine by a high viscous oil followed by a miscible oil displacement with n-decane, the oil relative permeability endpoint at irreducible water saturation was measured. This was used as reference for relative permeability normalization.

Numerical Simulations of Two-Phase Experiments

The two-phase experiments were selected in order to compare relative permeability from an analytical- and a numerical approach. A numerical simulator handling two-phase immiscible flow was used together with a Levenberg-Marquardt[19] algorithm (optimization scheme) to estimate the unknown relative permeabilities and capillary pressure functions. The relative permeabilities are represented by cubic B-splines with four interior knots and the capillary pressure by six interior knots. In all interior knots the resulting curves have a second order continuity and at the endpoints the knots are four fold. Confidence intervals are also included in the analysis.

DR1

It is impossible in general to find a parameter vector for which the simulator exactly reproduces the measurements. Since the Levenberg-Marquardt algorithm cannot differentiate between a global- and a local minimum of the object function, the final result will be influenced by the input functions. This was in particular seen when simulating the primary oil displacement (DR1). In this case a high viscous oil (72 cP) was displacing brine (1.06 cP). We expected a piston-like displacement for this situation, but as can be seen in Figure 5, a highly dispersed front was observed. A significant production also occurred after oil breakthrough. Furthermore, end-effects were present. Simulations of the DR1 experiment, using the analytical relative permeabilities and zero capillary pressure as input, failed to estimate the observed in-situ saturations, production curves and differential pressure observed during the experiment. Using the optimized capillary pressure in the same simulations did not improve the results. A check for the simulator performance was performed using relative permeabilities and capillary pressure data obtained by the optimization scheme as input. The results showed that the production data, differential pressure and the in-situ saturations all were reproduced by the simulator.

Without including a detailed dispersion analysis, this experiment seems to be influenced by capillary forces. An optimization analysis starting with different capillary pressure functions was performed to match the experiment and to obtain reasonable confidence intervals. The results were very sensitive to changes in capillary pressure. There was no difference in obtained functions and confidence interval using production/differential pressure data, and production/differential pressure/in-situ saturations data. We noted, however, that these results can be influenced by a scatter in the experimental in-situ saturation measurements. In this work, we have not used smoothed or synthetic experimental data and this may explain why the optimization

with only in-situ saturation data gave large confidence intervals, and a poor match to the production data.

Typical capillary pressure and relative permeability functions with 90 % confidence intervals are shown in Figures 2 and Figure 3, respectively. High viscous oil is the displacing fluid. We observed much larger confidence intervals in the oil-phase than in the water-phase. This may be because the oil mobility is quite insensitive to small perturbations in oil relative permeability due to high viscosity. In Figure 3 the optimized and analytical relative permeabilities are compared. Since capillary end-effects were present we would generally not expect these to be equal. The oil-phase, which has the largest confidence intervals, show most scatter in the relative permeability when the two methods are compared.

The obtained relative permeabilities and capillary pressure function from the optimization scheme were used as input in the simulation of the experiment. The simulated differential pressure is shown in Figure 4 and the corresponding in-situ saturation profiles are shown as dotted lines in Figure 5. The simulator was able to reproduce the dispersed fronts when using the optimized relative permeabilities and capillary pressure. The observed end-effects were not present in the simulations.

W1

From the obtained in-situ saturations, end-effects were minimal in the primary water-flood. However, the oil production curve from the analytical relative permeabilities failed to match the production curve from the experiment (Figure 6). A good agreement was obtained between the simulated production curves from the optimization scheme and the production and differential pressure from the experiment. Some end-effects were observed in the simulations, as seen in Figure 7. According to optimized capillary pressure, the water saturation has to be 0.4 at the outlet end before any production occurs. Water breakthrough occurred in both simulation and experimental data at 0.29 PV, but the water saturation at the outlet differ by about 0.2 (S_w =0.4 in simulations). The water front was quite smeared out in the simulations. A large scatter in permeabilities obtained by the two methods was also observed, but all the analytical relative permeabilities were within the 90 % confidence interval.

It will be noted that only production and differential pressure data were used in the optimization scheme. In the process, capillary pressure was adjusted (introducing capillary end-effects) to compensate for the smeared out front in order to match the observed breakthrough. The optimization scheme could not reproduce the experimental in-situ saturation data. Our conclusion here is that the obtained capillary pressure was not correctly estimated. (It should be noted that the capillary pressure analysis in W1 is not as rigorous as in DR1)

Summary

The simulation study has shown limitations in both the analytical- and the optimization approach to calculate relative permeabilities. In the W1 case we were able to see the limitations of an optimization scheme when using production and pressure data as input. The confidence intervals and fit to experimental data were good in the DR1 case. The observed dispersed front in the DR1 case can be explained in terms of frontal instabilities and viscous fingering which were not included in the simulation. Inspection of Figure 1 and simulations incorporating numerical dispersion support this view. Capillary pressure is interpreted as a second order diffusion term of the differential equation describing multi-phase flow in a porous medium. When the mathematical

model fails to describe the physical process, the relative permeability and capillary pressure functions become only adjustable parameters acounting for errors in the mathematical model. In our case frontal instabilities may explain the sensitivity for capillary pressure in DR1. However, scattering observed in the experimental data prevented further analysis.

Three-phase relative permeability

The end-effects observed from in-situ saturation plots of the three-phase experiments were minimal. Since to our knowledge, there is no published work on successful optimization schemes involving three-phase flow, only analytical relative permeabilities can be obtained.

Effects of a Free Gas Phase

Secondary gas injection, G2, after waterflooding resulted in a maximum gas saturation of about 36% pore volume. Gas trapping by waterflooding after gas injection can be compared from W3, W7, and W10 (Table 1). Only in W3 did the gas trapping initiate from a situation where the initial gas saturation was zero. The other data refer to increase in gas saturation above the level of trapped gas after several cycles of gas drainage and subsequent water imbibition. The trapped gas saturation is found to increase with increase in the initial gas saturation prior to the waterfloods.

The obtained trapped gas data are compared to the Land[12] equation proposed by Skauge et al using a Land constant of 1.9, see Figure 8. A Land coefficient of 3.0 would intercept the datapoints and thus, represent a best fit to the measurements. The trapped gas from this study show a sharper increase with initial gas saturation and does not fit a Land equation.

Residual Oil Saturation

Several experimental studies[11,13,14] have confirmed that the residual oil saturation in water-wet systems is lower in cores containing a trapped gas saturation during a waterflood compared to waterfloods with no trapped gas. The sum of trapped gas and residual oil in three-phase flow equals the two-phase waterflood residual saturation[11]. The residual oil and corresponding trapped gas are shown in Figure 9. The experimental data from the Clashach core is compared to relations between residual oil and trapped gas.

Influence of Gas Saturation on Oil and Water Relative Permeabilities.

Holmgren and Morse[13] found that the relative permeability to oil was significantly reduced by the presence of an immobile gas phase in a water-wet sandstone while water relative permeability was only slightly reduced. Schneider and Owens[15] concluded that for oil-wet cores, the presence of an immobile gas phase greatly reduced the water relative permeability, while the oil relative permeability was virtually unaffected. For the water-wet cores as used in this study, both water and oil relative permeabilities were reduced in the presence of an immobile gas phase. This is contrary to the findings of Holmgren and Morse in terms of the water relative permeability. More recent studies by Oak[16], and Skauge and Larsen[17] confirm the results of Holmgren and Morse[13]. The relative permeability of a wetting phase (water) depends most strongly on the saturation of that phase, and hysteresis is only a minor factor for the wetting phase. The oil drainage relative permeabilities show a large data scatter , and the relative permeabilities are generally somewhat higher than the values calculated from gas injection experiments. The oil relative permeability data show very little tendency to systematic changes with injected phase or

saturation history. The trend in the oil isoperms was a curvature concave towards oil for the water wet cores, as also has been concluded by others[16].

The shape of the gas relative permeability curves from constant pressure gradient experiments could indicate a functional representation independent of saturation. The gas relative permeability go to zero very abruptly, Figure 10. One attempt proposed earlier[17] to explain this unusual behavior is the suggestion of viscous fingering, i.e. gas bypassing a resident fluid (in this case oil and water). The gas would prefer to flow in the channels already occupied by gas, and the estimated relative permeability may become larger than "true" values, due to reduced pressure gradients after gas breakthrough. The gas relative permeability remains constant due to insignificant pressure drop by gas and nearly constant fractional flow after breakthrough.

The gas relative permeabilities show a strong dependence on process path i.e. increasing or decreasing saturation change, as observed in other experimental studies[16]. The gas relative permeability show no reduction in relative permeability due to different initial trapped gas saturation prior to the gas injection. This result is contradictory to observations by Skauge and Larsen[17].

Hysteresis in Relative Permeability Curves

Three-phase water relative permeabilities during gasflooding, Figure 11, is used to demonstrate water relative permeability hysteresis for this water-wet core. The curves as presented here display the initial water saturation and process part for each gasflooding cycle. When normalized to the same initial water saturation, the curves show indications that the three-phase water relative permeability is dependent only upon water saturation. Similar trends were observed in waterflood- and oilflood water relative permeabilities.

The plot of gas relative permeabilities as function of increasing gas saturation, Figure 10, indicates that gas relative permeabilities could be a function of gas saturation alone. A well defined set of oil relative permeabilities was observed during gasflooding cycles (Figure 12), but the oil drainage displacements show a considerable data scatter in the oil relative permeabilities; an aspect some researchers have termed a characteristic of three-phase relative permeability measurements. This is an indication that the three-phase oil relative permeability is dependent upon the saturation of the other phases. The work of Oak[16] and Narahara et al.[18] show that the three-phase relative permeabilities to oil, the intermediate phase, can be classified into two groups depending on whether the saturation was increasing or decreasing. The lack of repeatability in the oil relative permeabilities may be the result of random saturation change in our experiments as against a systematic saturation history variation used by Oak[16]. Our results emphasize the importance of considering hysteresis and saturation path in three-phase relative permeability measurements.

Conclusions

Results from three-phase relative permeability measurements show that the water relative permeability is depending on water saturation alone. There is no reduction in water relative permeability due to three-phase flow.

The presence of trapped gas reduce the residual oil saturation. The gas relative permeability appears to depend upon gas saturation alone at high gas saturations, but large uncertainty in gas relative permeability especially at low gas saturations prevent further analysis.

The oil phase relative permeability show considerable data scatter, which suggests that oil relative permeability may depend upon the saturation of the other phases.
Using in-situ saturations improve the interpretations of experiments for relative permeability calculations.

In order to reproduce production and differential pressure data from experiments, the optimization scheme to estimate relative permeability seems in this work superior to an analytical approach

Acknowledgements

This work received financial support from the Norwegian Research Council. The authors are grateful for the support

References

1. Lien, J.R., Graue, A., Kolltveit, K. "A Nuclear Imaging Technique for Studying Multiphase Flow in a Porou Medium at Oil Reservoir Conditions," Nuclear Instruments & Methods, **A271** 693-700, 1988.

2. Graue, A., Kolltveit, K., Lien, J.R., and Skauge, A.: "Imaging Fluid Saturation Development in Long Coreflood Displacements," SPEFE, Vol 5, No.4, (Dec. 1990), 406-412.

3. Skauge, A., Aanonsen, S.I., and Graue, A.: "Dynamic Fluid Saturation Profiles in the Analysis of Surfactant Flooding Core Displacement," SPE/DOE 17347, sixth Symp. on EOR, Tulsa, (April 1988), 289-302.

4. Eleri, O.O., Anowi, O., Graue, A., Skauge, A. and Kolltveit, K. "Nuclear Tracer Imaging of Fluid Saturations During Multiphase Flow in Porous Media," Sci./Tech. Report No. 1995-01, ISSN 0803-2696, Department of Physics, University of Bergen, Norway. (January 1995).

5. Rapoport, L.A., and Leas, W.A.: "Properties of Linear Water Floods," Trans. AIME (1953) 198, 139-148.

6. Virnovsky, G.A.: "Determination of Relative Permeability in a Three-Phase Flow in a Porous Media", translated from Iz 835-837

7. Grader, A.S., and O'Meara, D.J.: "Dynamic Displacement Measurements of Three-Phase Relative Permeabilities using Three Immiscible Liquids", SPE 18293, Presented at the 63rd Annual Technical Conference and Exhibition, Houston, Oct. 2-5, 1988.

8. Skauge, A. and Matre, B.: "Three Phase Relative Permeabilities in Brine - Oil - Microemulsion Systems," presented at the Fifth European Symposium on Improved Oil Recovery, Budapest, (April 1989), 473-483.

9. Kvanvik, B.A., Skauge, A., Matre, B., and Kolltveit, K.: "Three-Phase Microemulsion Relative Permeability- Experimental and Theoretical Considerations," presented at the Sixth European Symposium on Improved Oil Recovery, Stavanger, (May 1991), published in Journal of Petroleum Science and Engineering, Vol 7, (1992) 105-116.

10. Olsen, G., Skauge, A., and Stensen, J.Å.: "Evaluation of the Potential Application of the WAG Process in a North Sea Reservoir," presented at the Sixth European Symposium on Improved Oil Recovery, Stavanger, (May 1991), published in the Revue de l'Institut Francais du Petrole, Jan.-Febr. (1992) 81-93.

11. Skauge, A. and Aarra, M.: "Effect of Wettability on the Oil Recovery by WAG", presented at the 7th European IOR-Symposium in Moscow, Oct 26-28, 1993, proceedings Vol 2, 452-458.

12. Land, C.S.: "Calculation of Imbibition Relative Permeability for Two- and Three -Phase Flow from Rock Properties," SPEJ, 149-156, June 1968

13. Holmgren, C.R., and Morse, R.A.: "Effect of Free Gas Saturation on Oil Recovery by Waterflooding," Trans. AIME (1951) 192, 134-140

14. Kortekaas, T.F.M., and van Poelgeest, F.: "Liberation of Solution Gas during Pressure Depletion of Virgin and Watered-out Oil Reservoirs," SPERE, (Aug. 1991) 329-335.

15. Schneider, F.N., and Owens, W.W.: "Sandstone and Carbonate Two- and Three-Phase Relative Permeability Characteristics," SPEJ (March 1970) 75-84

16. Oak, M.J.: "Three-Phase Relative Permeability of Water-Wet Berea," paper SPE/DOE 20183 presented at the 1990 Symposium on EOR, Tulsa, April 22-25.

17. Skauge, A., and Larsen, J.A.: "Three-Phase Relative Permeabilities and Trapped Gas Measurements Related to WAG Processes," presented at the1994 International Symposium of the Society of Core Analysists, Stavanger, September 12-14, 1994, proceeding paper SCA 9421.

18. Narahara,G.M., Pozzi, A.L., and Blackshear, T.H.: Effect of Connate Water on Gas/Oil Relative Permeabilities for Water-Wet and Mixed-Wet Berea Rock," SPE 20503, SPE Annual Tech. Conf. and Exh., New Orleans, (Sept. 1990

19. Gill, Murray, Wright. "Practical Optimization," Academic press inc. (1981)

Table 1 Summary of Saturation History During Displacement Sequences

	Initial			End-point			
Exp	Sw	So	Sg	Sw	So	Sg	kri
DR1	1.00	0.00	0.00	0.21	0.79	0.00	1.00
W1	0.21	0.79	0.00	0.54	0.46	0.00	0.12
G2	0.54	0.46	0.00	0.35	0.29	0.36	0.39
W3	0.35	0.29	0.36	0.63	0.23	0.14	0.13
O4	0.63	0.23	0.14	0.32	0.55	0.13	0.43
W5	0.32	0.55	0.13	0.48	0.42	0.10	0.10
G6	0.48	0.42	0.10	0.34	0.24	0.41	0.39
W7	0.34	0.24	0.41	0.67	0.15	0.18	0.12
O8	0.67	0.15	0.18	0.34	0.54	0.12	0.22
G9	0.34	0.54	0.12	0.28	0.27	0.45	0.39
W10	0.28	0.27	0.45	0.63	0.16	0.22	0.12
O11	0.63	0.16	0.22	0.24	0.76	0.01	0.66
W12	0.24	0.76	0.01	0.52	0.47	0.01	0.10

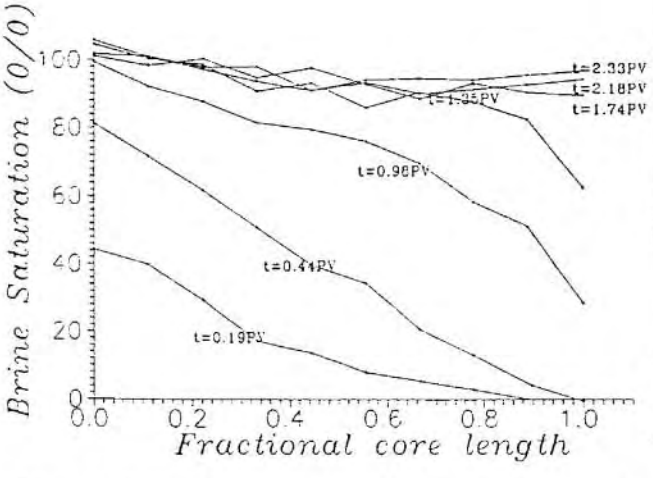

Figure 1 Miscible displacement
(tagged brine displacing brine)

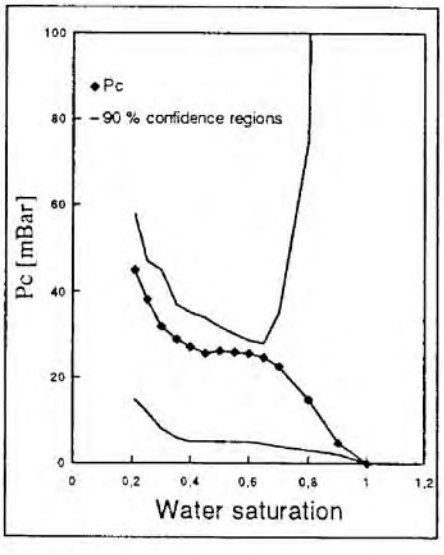

Figure 2 Capillary pressure from DR1

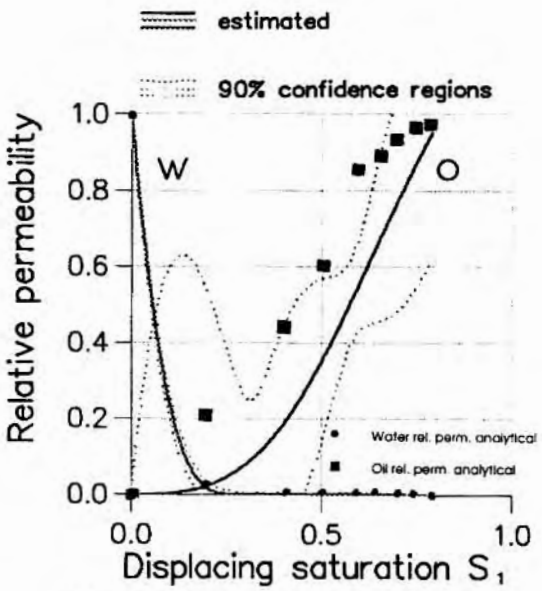

Figure 3 Numerical- and analytical relative permeability obtained from DR1

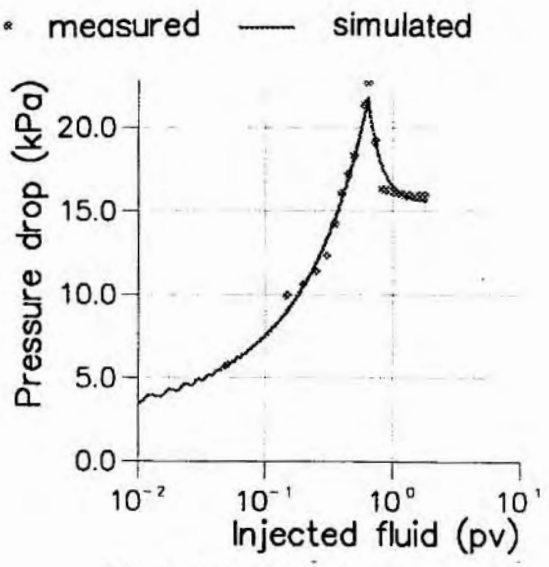

Figure 4 Differential pressure, DR1

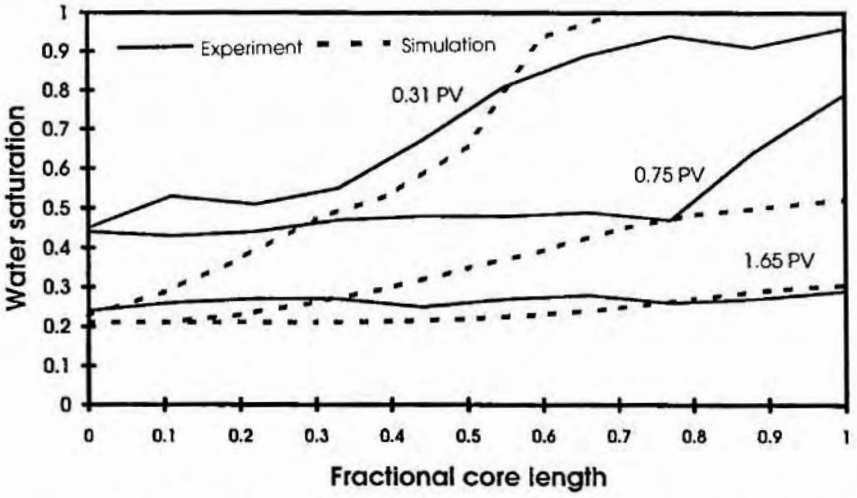

Figure 5 In-situ saturation from DR1, experiment and simulation

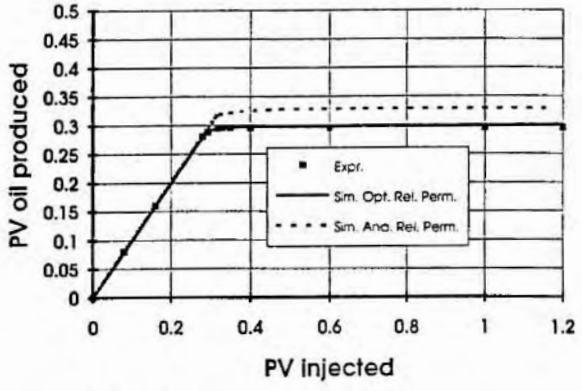

Figure 6 Oil production, W1

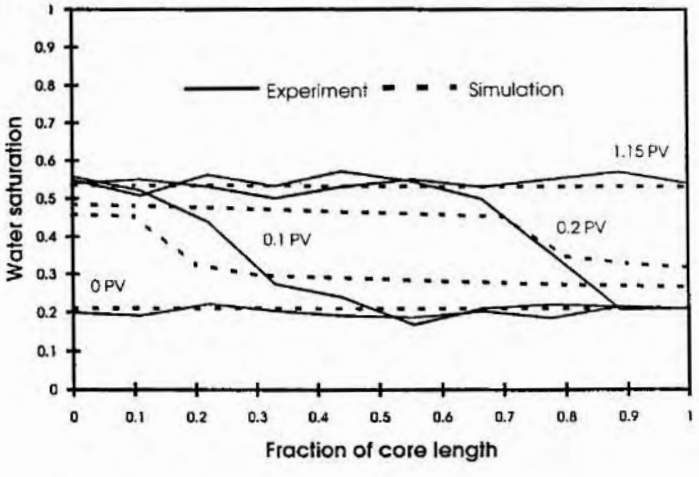

Figure 7 In-situ saturations from W1, experiment and simulation

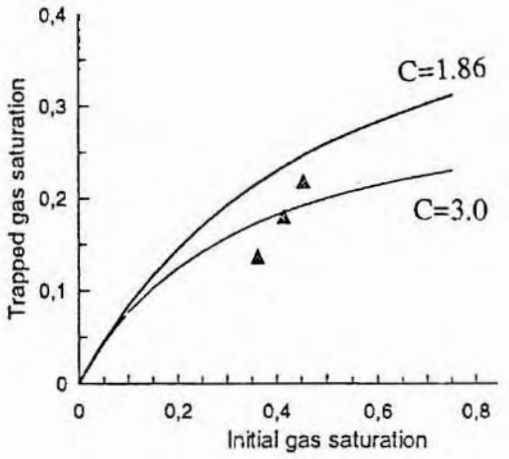

Figure 8. Trapped gas saturation compared to a proposed Land equation from ref. 11.

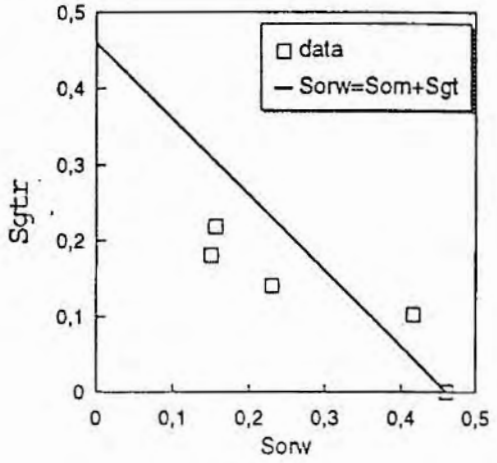

Figure 9. Relationship between trapped gas and residual oil saturation

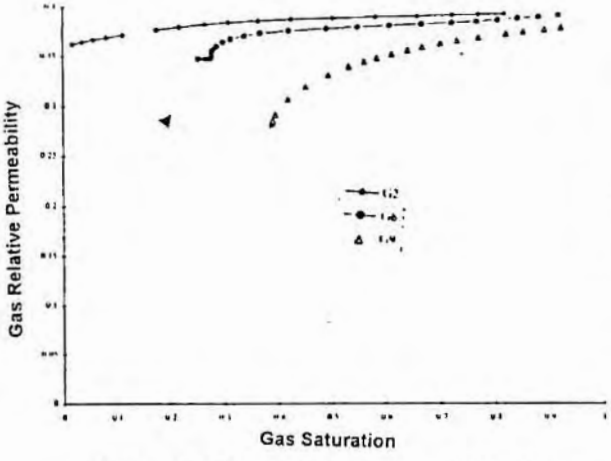

Figure 10. Gas relative permeability from const. differential pressure gas injections

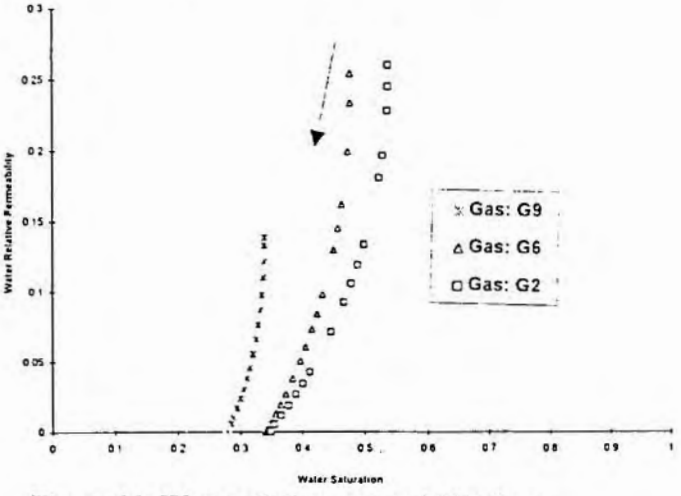

Figure 11. Water relative permeability from const. differential pressure gas injections

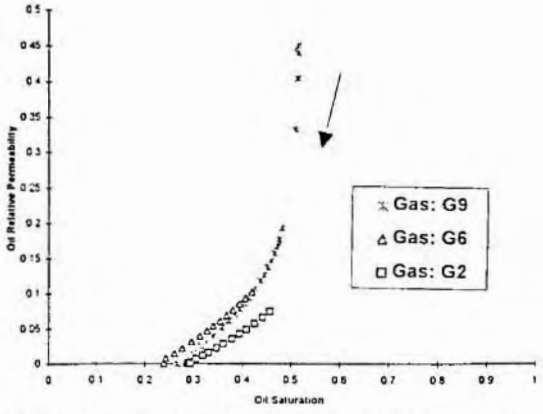

Figure 12. Oil relative permeability from drainage by oil injection.